Dynamics of Two Planets in the 2/1 Mean-Motion Resonance

N. Callegari Jr., T. A. Michtchenko, S. Ferraz-Mello
Instituto de Astronomia, Geofísica e Ciências Atmosféricas
Universidade de São Paulo, Brasil

Abstract

The dynamics of two planets near a first-order mean-motion resonance is modeled in the domain of the general three-body planar problem. The system studied is the pair Uranus-Neptune (2/1 resonance). The phase space of the resonance and near-resonance regions is studied by means of surfaces of section and spectral analysis techniques. After a thorough investigation of the topology of the phase space, we find that several regimes of motion are possible for the Uranus-Neptune system, and the regions of transition between the regimes of motion are the seats of chaotic motion.

1 Introduction

Until recently, researches considering the long-term stability of planetary systems were based on the studies of the dynamics of the nine planets of our Solar System and the orbital evolution of the massive satellites of the giant planets. These studies were performed in different ways through the solutions of averaged models (Sessin and Ferraz-Mello 1984, Hadjidemetriou 1985, Laskar 1989, Gladman 1993, Michtchenko and Ferraz-Mello 2001a, hereafter MF2001a), or long numerical integrations of the equations of motion of these systems (Sussman and Wisdom 1988, Nobili *et al.* 1989, Lecar *et al.* 2001, Michtchenko and Ferraz-Mello 2001b, hereafter MF2001b). In present day, however, the discovery of a great number of extra-solar planets has increased the domain of these investigations.

One of the main reasons for this new interest is that some systems including more than one planet are actually in resonant orbital configurations. In this situation, the mean motion of two planets are commensurable. In the Solar planetary system, three near mean-motion resonances occur: the 5/2 near-resonance in Jupiter-Saturn system, the 3/1 near-resonance in Saturn-Uranus system, and the 2/1 near-resonance in the Uranus-Neptune. Among the known extra-solar planets, we can cite several examples of systems in near resonant configuration. In the case of planetary systems in near *first-order* mean-motion resonances, one example is the pair B-C of the planetary system orbiting the pulsar PSR B1257+12 (Wolszczan and Frail 1992). In this system, the two planets are close to the 3/2 near-resonance. Some studies were performed on the long-term stability of this system through simplified models (Rasio *et al.* 1992, Malhotra *et al.* 1992). Another example is the 2/1 resonant pair of planets orbiting the star Gliese 876 recently discovered (Marcy *et al.* 2001). The third example is of the star HD 82943, which also has two planets close to 2/1 mean-motion resonance (Israelinan *et al.* 2001). The stability of these systems has been studied by several authors (Kinoshita and Nakai 2001, Lee and Peale

2002, Hadjidemetriou 2002). Beyond the first order resonances, there are some pairs in high-order resonances (55Cnc, 47 Uma, etc). Another important dynamical property of planetary systems related with the results shown in this paper, is the presence of secular locking of the line of apses (Milani and Nobili 1984, Malhotra 2002, Michtchenko and Malhotra 2004).

In fact, resonant configuration and secular apses alignment in planetary systems may be a rule and not an exception (see Malhotra 1998). In spite of some recent developments, the dynamics of the near resonant configuration in planetary systems is still poorly understood (Tittemore and Wisdom 1988, hereafter TW1988, Varadi *et al.* 1999, Murray and Holman 1999, MF2001a,b). This is the main motivation of this work. We consider in this paper the case of the 2/1 planetary mean-motion resonance. The investigation is done with the help of a general averaged planar two-degrees-of-freedom Hamiltonian model (Section 2). The model is applied to the study of the 2/1 near-resonance in the Uranus-Neptune system. The choice of initial conditions is described in detail in Section 3. The main regimes of motion of the system obtained over a large set of initial conditions by means of surfaces of section and spectral map techniques are described in Section 4 (the kernel of this paper). In Section 5, the results of the study of the 2/1 resonance are summarized on the plane defined by two free parameters of the problem under study. Finally, the conclusions and discussion are given in the Section 6.

2 The model

Consider a pair of planets with finite masses m_1 and m_2 orbiting a central star m_0 (hereafter the indexes 0, 1 and 2 refer to the central star, inner and outer planets, respectively). Suppose that the orbital periods of the planets are close to the commensurability $(p+q)/p$, where p and q are small integer. In this work, our model is applied to the study of the Uranus-Neptune planetary system which is close to the 2/1 mean-motion resonance.

In order to construct the Hamiltonian of such system, we use the canonical set of heliocentric variables introduced by Poincaré (Poincaré 1897, Hori 1985, Laskar and Robutel 1995). Let $\vec{u}_i$ and $\vec{p_i}= m_i\frac{d\vec{u}_i}{dt}$ $(i = 0, 1, 2)$ be the position and the momentum vectors of the bodies relative to center of the mass of the system, and $\vec{r_i}=\vec{u_i} - \vec{u_0}$ be the position vectors of the planets relative to the central star. In the Poincaré system, the canonical variables are given by the pairs $(\vec{r_i}, \vec{p_i})$, and the exact Hamiltonian of the problem is written as

$$H = \sum_{i=1}^{2}\left(\frac{|\vec{p_i}|^2}{2\beta_i} - \frac{\mu_i\beta_i}{|\vec{r}_i|}\right) - G\frac{m_1m_2}{\Delta_{12}} + \frac{\vec{p_1}\cdot\vec{p_2}}{m_0}, \qquad (1)$$

where

$$\mu_i = G(m_0 + m_i), \qquad \beta_i = \frac{m_0m_i}{m_0 + m_i}.$$

G is the gravitational constant and $\Delta_{12} = |\vec{r_1} - \vec{r_2}|$ is the distance between planets.

The first term of the Hamiltonian (1) defines unperturbed Keplerian motion of the planets around the star. The second and third terms are the perturbation due to the mutual attraction between the planets; these terms will be called hereafter as direct and indirect parts of the Hamiltonian, respectively.

We introduce the Poincaré variables:

$$\begin{aligned} L_i &= \beta_i\sqrt{\mu_i a_i}, & \lambda_i;\\ L_i - G_i &= L_i(1 - \sqrt{1 - e_i^2}), & -\varpi_i;\\ G_i - H_i &= L_i\sqrt{1 - e_i^2}(1 - \cos I_i), & -\Omega_i, \end{aligned} \qquad (2)$$

where a_i, e_i, I_i, λ_i, ϖ_i, Ω_i are the planetary semi-major axes, eccentricities, inclinations, mean longitudes, longitudes of perihelion and longitudes of nodes associated with the Keplerian part of the Hamiltonian (1). It should be emphasized that these elements describe instantaneous ellipses which intersect the trajectories, in contrast with the familiar heliocentric osculating orbits, which are tangent to them (for more details, see Ferraz-Mello *et al.* 2004).

In the variables given by eq. (2), the Hamiltonian (1) can be written as

$$H = H_0 + H_1, \tag{3}$$

where the Keplerian part is given by

$$H_0 = -\sum_{i=1}^{2} \frac{\mu_i^2 \beta_i^3}{2L_i^2}, \tag{4}$$

and the mutual terms are given by the disturbing function

$$H_1 = -\frac{Gm_1m_2}{a_2} \times R(\lambda_i, \varpi_i, \Omega_i, L_i, L_i - G_i, G_i - H_i). \tag{5}$$

In order to study the secular and resonant dynamics of the planets, we expand the function R in powers of eccentricities and inclinations of both planets (Le Verrier 1855). Since the inclinations of the orbits of Uranus and Neptune are small, we restrict our model to the planar case. In the planar expansion of R, we keep the main second-degree secular terms and the resonant terms up to second order in eccentricities. Higher-degree secular terms are omitted since their contribution is not important (MF2001a). The short-period terms of order of orbital periods are removed from R through a first-order averaging, and therefore only the long period and resonant terms remain.

With the approximations done, the mutual part (5) is given by

$$H_1 = H_{\rm sec} + H_{\rm res}, \tag{6}$$

where

$$H_{\rm sec} = -\frac{Gm_1m_2}{a_2}\left[a + b(\frac{e_1^2}{2} + \frac{e_2^2}{2}) + c(\frac{e_1}{2})(\frac{e_2}{2})\cos(\varpi_1 - \varpi_2)\right] \tag{7}$$

and

$$\begin{aligned} H_{\rm res} \;=\; & -\tfrac{Gm_1m_2}{a_2}\{d\,(\tfrac{e_1}{2})\cos[(1+r)\lambda_2 - r\lambda_1 - \varpi_1] \\ & + e\,(\tfrac{e_2}{2})\cos[(1+r)\lambda_2 - r\lambda_1 - \varpi_2] \\ & + f\,(\tfrac{e_1^2}{2})\cos 2[(1+r)\lambda_2 - r\lambda_1 - \varpi_1] \\ & + g\,(\tfrac{e_2^2}{2})\cos 2[(1+r)\lambda_2 - r\lambda_1 - \varpi_2] \\ & + h\,(\tfrac{e_1}{2})(\tfrac{e_2}{2})\cos 2[(1+r)\lambda_2 - r\lambda_1 - \tfrac{1}{2}\varpi_1 - \tfrac{1}{2}\varpi_2]\}. \end{aligned} \tag{8}$$

For the 2/1 resonance, $r = p/q$ and $p = q = 1$. The coefficients a, b, c, d, e, f, g, h are functions of the semi-major axes ratio $\alpha = a_1/a_2$, and are given in the Appendix. In the case of the 2/1 resonance, the indirect part of the Hamiltonian (1) contributes with a single term, which must be included in the coefficient e; its expression is given in eq. (15) in the Appendix.

New resonant variables may be introduced through the canonical transformation:

$$\begin{aligned} I_1 &= L_1 - G_1, & \sigma_1 &= (1+r)\lambda_2 - r\lambda_1 - \varpi_1; \\ I_2 &= L_2 - G_2, & \sigma_2 &= (1+r)\lambda_2 - r\lambda_1 - \varpi_2; \\ J_1 &= L_1 + r(I_1+I_2), & & \lambda_1; \\ J_2 &= L_2 - (r+1)(I_1+I_2), & & \lambda_2. \end{aligned} \tag{9}$$

In terms of these variables, the averaged Hamiltonian is cyclic in λ_1 and λ_2 and, consequently, J_1 and J_2 are constants of motion. The system is reduced to a system with two degrees of freedom, whose variables are σ_1, σ_2, I_1 and I_2. The constants J_1 and J_2 appear in the Hamiltonian through L_1 and L_2.

From (9), we can note that

$$(1+r)L_1 + rL_2 = (1+r)J_1 + rJ_2 = const,$$

that is, the resonant variations of the averaged semi-major axes are coupled in such a way that the increase of one of them implies, necessarily, in the decrease of the other. Also, the amplitudes of the semi-major axes oscillations are inversely proportional to the planetary masses (MF2001a).

Assuming that for small eccentricities, $I_i \approx J_i \frac{e_i^2}{2}$, we expand H in a double series of I_i, $i = 1, 2$. The constant terms in the expansion can be omitted and the Hamiltonian (3) is then written as

$$\begin{aligned} H &= 2A(I_1+I_2) + 4B(I_1+I_2)^2 + \\ &\quad 2CI_1 + 2DI_2 + 2E\sqrt{I_1 I_2}\cos(\sigma_1 - \sigma_2) + \\ &\quad F\sqrt{2I_1}\cos\sigma_1 + I\sqrt{2I_2}\cos\sigma_2 + \\ &\quad 2RI_1\cos 2\sigma_1 + 2SI_2\cos 2\sigma_2 + \\ &\quad 2T\sqrt{I_1 I_2}\cos(\sigma_1 + \sigma_2), \end{aligned} \tag{10}$$

where the expressions and numerical values of the coefficients are given in the Appendix. The units chosen in this work are the mass of the central body (Sun), astronomical unit and year.

The terms with coefficients A and B in eq. (10) arrive from the Keplerian parts of Hamiltonian (4) and are of degree 2 and 4 in the eccentricities, respectively. The terms with coefficients C, D and E come from both the secular $H_{\rm sec}$ (7) and Keplerian part (4) and are of degree 2 in the eccentricities. Finally, the other terms come from $H_{\rm res}$ and are the main resonant terms (F, I) of degree 1 in eccentricities and their second harmonics (R, S and T).

2.1 The choice of the constants of motion J_1 and J_2

The coefficients of the Hamiltonian (10) are functions of the two constants J_1 and J_2, which are known from initial conditions through eqs. (9). In this work, we replace these quantities by constant J_{10} and J_{20}, which can be calculated by setting $e_1 = e_2 = 0$ and $L_{i0} = \beta_i\sqrt{\mu_i a_{i0}}$, $i = 1, 2$. The choice of the semi-major axes with indices 0 is done fixing the semi-major axis of one of the planets and calculating the other through equation:

$$\alpha_0 = \frac{a_{10}}{a_{20}} = \left(\frac{m_1+m_0}{m_2+m_0}\right)^{\frac{1}{3}}\left(\frac{r}{1+r}\right)^{\frac{2}{3}},$$

where α_0 is the ratio of the planetary semi-major axes at the exact resonance. For our purpose, we fix the semi-major axis of Neptune at its time averaged value obtained from a numerical integration of the exact equations of motion over 5Myr. The numerical values of a_{10}, a_{20}, J_{10}, and J_{20} used in the present investigations, are given in Table II in the Appendix.

Our previous study has shown that the variation of the numerical values of the coefficients of the Hamiltonian (10) is very small when the constants J_1, J_2 and the Laplace coefficients are calculated outside the exact resonance. In this way the given approximation is realistic over the domain under investigation.

2.2 The parameter δ

Once the ratio of a_{10} and a_{20} is kept in the neighborhood of the exact resonance value α_0, the numerical values of the coefficients B, C, D, E, F, I, R, S, T of the Hamiltonian (10) depend weakly on the initial semi-major axes and eccentricities. These coefficients appear in eq. (10) multiplied by a power of I_i and the variations of the coefficients affect our equations only slightly. The same is not true for the coefficient A. Indeed, we can deduce that, in the proximity of resonance and for small eccentricities, $A \sim \frac{1}{2}[(1+r)\,n_2 - r\,n_1]$, where n_i are the mean motions of the planets. This expression is a resonant combination of the planetary mean motions and, consequently, A is very sensitive to the adopted initial conditions. In order to study our system in several initial conditions and not only in the exact resonance, we introduce the parameter

$$\delta \equiv 2(A + C),$$

which, in the first approximation, can be written as $\delta \approx (1+r)\,n_2 - r\,n_1 - \dot{\varpi}_1$.

In this work, the coefficients B, C, D, E, F, I, R, S, T are fixed at the values calculated with J_{10} and J_{20} using eqs. (16) in the Appendix. The values obtained are shown in Table III in the Appendix. In order to describe the planetary dynamics in the neighborhood of the 2/1 resonance, only the parameter δ is changed. In Section 4, we present the results of investigations done with $\delta = 0.0012$, which is close to the actual value of the pair Uranus-Neptune, ($\delta \approx 0.0015$). The solutions obtained for different values of δ are present in Section 5.

To prevent from the appearance of zero divisors, it is convenient to write the Hamiltonian given by eq. (10) in the non-singular canonical variables $x_i = \sqrt{2I_i}\cos\sigma_i$, $y_i = \sqrt{2I_i}\sin\sigma_i$, where $i = 1, 2$. In these variables, the Hamiltonian (10) is written as:

$$\begin{aligned} H \;=\; & B(x_1^2 + y_1^2 + x_2^2 + y_2^2)^2 + \\ & \frac{1}{2}(\delta - 2C)(x_1^2 + y_1^2 + x_2^2 + y_2^2) + \\ & C(x_1^2 + y_1^2) + D(x_2^2 + y_2^2) + E(x_1x_2 + y_1y_2) + \\ & Fx_1 + Ix_2 + \\ & R(x_1^2 - y_1^2) + S(x_2^2 - y_2^2) + T(x_1x_2 - y_1y_2). \end{aligned} \tag{11}$$

It should be emphasized that the Hamiltonian given by eqs. (10) or (11) is valid only for small values of the planetary eccentricities.

3 Representative plane of initial conditions

Let us now discuss the problem of the choice of the initial conditions: the initial eccentricities and critical angles σ_1 and σ_2. The study of the dynamics of the system requires an analysis in a four-dimensional space of initial conditions ($e_1, e_2, \sigma_1, \sigma_2$). In this work, we restrict the set of initial conditions fixing the initial values of angular variables at $\sigma_i = 0$ or π, $i = 1, 2$. It is important to note that with this restriction, the solutions in the neighborhood of asymmetric stable equilibrium points of the averaged system (Beaugé 1994, Beaugé *et al.* 2002, Ferraz-Mello 2002, Ferraz-Mello *et al.* 2003) are not considered.

With the choice $\sigma_i = 0$ and π, we have $y_i = \sqrt{2I_i}\sin\sigma_i = 0$. The Hamiltonian H is a quartic polynomial with respect to $x_i = \sqrt{2I_i(e_i)}\cos\sigma_i$. The set of initial conditions belongs now to the plane (e_1,e_2) and can be studied by plotting the level curves of the Hamiltonian (11) on this representative plane. The energy levels of $H = f(x_1(e_1), x_2(e_2); \delta)$ calculated with $\delta = 0.0012$ are shown in Fig. 1.

Since H is a quartic polynomial in the eccentricities, there may exist up to four real roots of the eccentricity of the outer planet (e_2), for given values of H, δ, and e_1. These roots can be organized in a convenient way. When they are all real, we sort them in order of increasing value

and denote them by the letters a, b, c and d, respectively. In this case, the pairs b,c and a,d are called inner and outer pair, respectively. When one pair of the roots is not real, the simplest way of sorting is attributing zero value for its real part, and to proceed as in the case of four real roots. We then choose one of the real roots as the initial condition, and solve the canonical equations of motion numerically using the integrator RA15 (Everhart 1985).

The problem, now, is the choice of one of the roots for the construction of the surfaces of section. We can divide this problem into two parts. First, let us consider all energy levels that are located *outside* the "banana" curve in Fig. 1 (regions 1 and 2). Based on the numerical experiments, we can state that, in this case, the dynamics of the system is similar, no matter which root is chosen (a, b, c or d; see MF2001a). Let us now consider the levels indicated by the letters *b, c, d,..., l* inside the "banana" curve in Fig. 1 (region 3). Again, based on several numerical tests, we have that for these energies, the roots a and b provide the most general information on the global dynamics of the system. In other words, would one of the roots c or d be chosen, many information revealed by the root a and b would be lost, as we will see in Section 4. In fact, in Sections 4.6 and 4.7, we will deal, in detail, with this important aspect of the phase space, and an example showing the four sections will be given Section 4.6. The complete atlas of sections can be found in Callegari (2003) (see also Section 3 of TW1988).

Depending on δ, the number of the zero-gradient points on the representative plane varies from one to three. For the δ value used in the construction of Fig. 1, there are three points where the gradient of $H = f(e_1, e_2; \delta)$ is zero: the saddle point PII$^-$, the point C corresponding to a local minimum of energy ($H_{\min}$), and the stable equilibrium point PII$^+$ corresponding to a maximum of energy H(PII$^+$). The plane of initial conditions can be divided into three distinct regions. For $H < H_{\min}$ and a given e_1, there exist always two real roots e_2 (dashed curves in region 1). For $H_{\min} \leq H < H$(PII$^-$) (region 2), there may exist two or four real roots. Finally, for H(PII$^-$) $\leq H \leq H$(PII$^+$) (region 3), two, four or no real roots e_2 exist for a given e_1. In all these cases, double real roots are also possible. For levels $H > H$(PII$^+$), no real roots are possible, since PII$^+$ is the point of the maximum energy.

The region 1 is dominated by purely secular interactions between the planets. The region 2 is a near-resonance zone which can be subdivided into inner and outer domains. The inner near-resonance domain is characterized by a prograde circulation of the critical angles σ_1 and σ_2. In the outer near-resonance domain, σ_1 and σ_2 are in a retrograde circulation. Finally, the region 3 is called resonance zone, since, as we will see in the next section, the main features of the 2/1 resonance appear when these energies are reached.

The thick curves in Fig. 1 define the location of the periodic solutions on the plane (e_1, e_2) given by conditions:

$$\begin{aligned} \frac{d\sigma_1}{dt} &= \frac{\partial H}{\partial I_1} = 0 \\ \frac{d\sigma_2}{dt} &= \frac{\partial H}{\partial I_2} = 0. \end{aligned} \tag{12}$$

These curves must intercept themselves in the zero-gradient points of $H = f(e_1, e_2)$ (the points PII$^-$, PII$^+$ and C), and will be used in the construction of the parameter plane in Section 5.

4 Dynamics of the 2/1 planetary resonance

In this section, we present a study of the dynamics of the system defined by eq. (11) using surfaces of section and spectral analysis techniques.

The surfaces of section of planetary motion are introduced as follows. The inner planet section (Uranus section) is defined by the condition $y_2 = 0$ and represented on the plane ($e_1 \cos \Delta\varpi \times e_1 \sin \Delta\varpi$), where $\Delta\varpi = \sigma_1 - \sigma_2 = \varpi_2 - \varpi_1$. The outer planet section (Neptune section) is defined

Level/Figure	Energy ($\times 10^{-9}$)	Regimes of motion
a/Fig. 2 a	1.3	MI, MII
b/Fig. 2 b	1.33622	MI, MII $\rightarrow$ RIII
c/Fig. 6 a	1.34	MI, RIII
d/Fig. 6 b	1.36	MI, RIII
e/Fig. 6 c	1.40	MI, RIII
f/Fig. 6 d	1.45	MI, RIII
g/Fig. 8 a	1.46	MI, RIII, RIV
h/Fig. 8 b	1.4985	MI, RIII, RIV
i/Fig. 9	1.51	MI, RIII, RIV
j/Fig. 12	1.523	RIII, RIV, RV
k/Fig. 13 a	1.55	MI, RIV
l/Fig. 13 b	1.90	RIV

Table 1: Energy levels used in the construction of the surfaces of sections and the regimes of motion present on the corresponding section.

by condition $y_1 = 0$ and represented on the plane ($e_2 \cos \Delta\varpi \times e_2 \sin \Delta\varpi$). It should be emphasized that the two sections are mathematically equivalent. However, for a better interpretation of the results, both sections are shown in this paper.

In the construction of the sections, we use generally the root $\underline{a}$ of eq. (11) described in Section 3. As the Hamiltonian (11) is quartic with respect to x_i, to construct the surfaces of sections, we need to fix two additional conditions. These conditions were obtained from our previous numerical experiments, in such a way that, for the inner planet section, $\frac{dy_2}{dt} > 0$ and $x_2 < 0$ ($\sigma_2 = \pi$). For the outer planet section, $\frac{dy_1}{dt} < 0$ and $x_1 > 0$ ($\sigma_1 = 0$). The root $\underline{b}$ of eq. (11) was used only in the construction of the sections present in Sections 4.6 and 4.7. In that case, we use $\frac{dy_2}{dt} < 0$ and $x_2 < 0$ ($\sigma_2 = \pi$), for the inner planet section, and $\frac{dy_1}{dt} > 0$ and $x_1 > 0$ ($\sigma_1 = 0$), for the outer planet sections.

Another technique used in this work is the spectral analysis of the solutions shown on the Uranus sections. For each initial condition, the system of the canonical equations of motion is numerically integrated and the solution obtained is Fourier analyzed. The frequencies present in the oscillation of the variable x_1 with amplitudes greater than 1% of the largest peak are plotted in the spectral map. For a better resolution, we use a logarithmic scale. Since the Hamiltonian system under study has two degrees of freedom, we expect to obtain two fundamental frequencies, as well as their higher harmonics and linear combinations. The spectra of regular solutions show generally a few significant peaks associated with the independent frequencies and their linear combinations. The spectra of chaotic motion show broadband components. Thus, the spectral analysis technique is complementary to the surfaces of sections and allows us to distinguish between regular and chaotic motion.

Table I shows the energy levels which have been used in the study of the phase space of the 2/1 planetary resonance. The first column of Table I shows the letter of the corresponding level in Fig. 1 (*a, b, c, d,..., l*), together with the number of the figure containing the corresponding surface of section. The second column shows the value of the energy level. Finally, the third column displays the regimes of motion which have been detected at the corresponding energy level.

As the energy is increased, the system passes through several types of motion. Here, we

summarize briefly the results of our investigations, which will be discussed in detail in the next sections. One of the regimes detected is a secular motion in the near-resonance region; this regime is denoted by MI or MII in Table I. The other regimes of motion are related to the different types of motion inside the 2/1 resonance. They are denoted by RIII, RIV and RV in Table I. Each regime of motion is characterized by its periodic solution, which appears as a fixed point on the surface of section. The domain of one regime of motion is separated from the other regions by layers of chaotic motion. In all figures shown in the following sections, the top and middle figures represent the inner and outer planet surfaces of section, respectively. The bottom figures show the corresponding spectral maps. The bold curves on the surfaces of section are the boundaries of the energy manifold: outside these curves, the quartic polynomial given by the Hamiltonian (11) does not have real solutions.

4.1 Secular Modes

We begin our analysis of the dynamics of the 2/1 resonance showing the surfaces of section obtained along the energy level a in Fig. 1. The corresponding surfaces of section and spectral maps are shown in Fig. 2a. At this energy, the system is outside the 2/1 resonance and its dynamics is dominated by secular interactions. In this near-resonance zone, the dynamics of the system is characterized by two secular modes of motion known from the linear secular theories (see Pauwels 1983, TW1988, MF2001a). There are two periodic solutions: one is given by $\Delta\varpi = \sigma_1 - \sigma_2 = 0$ and another by $\Delta\varpi = \pm\pi$. Hereafter we designate the solutions at $\Delta\varpi = 0$ as Mode I of motion and those at $\Delta\varpi = \pm\pi$ as Mode II. On the surfaces of section in Fig. 2a, the Mode I of motion is always located on the right-hand side of the sections, while the Mode II is located on the left-hand side. The smooth curves surrounding each of the two fixed points are quasi-periodic solutions.

In this paper, we describe briefly our results concerning the secular modes (for the complete study, see MF2001a, Callegari 2003, Michtchenko and Malhotra 2004). Deeply inside Mode I, the angle $\Delta\varpi$ oscillates around 0, while inside Mode II, $\Delta\varpi$ oscillates around π; in both cases the eccentricity of the planets vary regularly around the values of the periodic orbits. Between the Modes I and II, the angle $\Delta\varpi$ is in a prograde circulation, and the motion is a composition of the two normal modes. The secular oscillations of the eccentricities always occur with opposite phases: when the eccentricity of the outer planet e_2 is minimal, the eccentricity of the inner planet e_1 is maximal. Conversely, when the eccentricity e_2 is maximal, e_1 is minimal.

It has been shown in MF2001a that, in the near-resonance zone, the motion of the critical angles σ_1, σ_2 is a direct (C_D) or a retrograde circulation (C_R), depending on the initial conditions. The direct circulation corresponds to the inner pair of the roots (b or c) of eq. (11), while the retrograde circulation corresponds to the outer pair of roots (a or d). As we are working with the root a, σ_1 and σ_2 are in a retrograde circulation in both modes (C_R).

In the near-resonance zone, there is no real separatrix between the two modes of motion on the surfaces of section, and the motion is always regular (MF2001a). Indeed, the spectral map present at the bottom of Fig. 2a shows the continuous evolution of the two fundamental frequencies and their harmonics. Around Mode I of motion, the secular period of the system is 400,000 years, while around Mode II it is approximately 300,000 years. We can see that, for the initial condition near the fixed points, the amplitude of the secular frequency is equal to zero. The other frequency, which can also be seen in the spectral map in Fig. 2a, is the frequency associated with the circulation of the critical angles (second fundamental frequency). It is located in the upper part of the spectral map.

4.2 The onset of chaos at the center of Mode II

The energy level shown in Fig. 2b corresponds to the curve b in Fig. 1. For initial conditions in the neighborhood of the point PII^-, the system is at the edge of the resonance zone. The regular behavior of the system suffers qualitative changes. Note that these changes cannot be

seen on the surfaces of section in Fig. 2b, where all solutions are apparently regular. However, they are clearly visible in the spectral map near the center of Mode II. The evolution of the main frequencies around the fixed point of Mode II is characterized, now, by an erratic scatter of the points, which is associated with chaotic behavior of trajectories close to a separatrix.

Figure 3 shows a detail of the region of the representative plane (e_1,e_2) around the equilibrium point PII$^-$. In this region, the critical angles alternate between direct and retrograde circulation, and this fact explains the chaotic behavior indicated by the spectral map. In order to illustrate this transition motion of the critical angles, we present in Fig. 4 the planetary trajectories calculated for one initial condition very close to the point PII$^-$. The critical angle of Uranus changes alternately between direct (C_D) and retrograde (C_R) circulation (Fig. 4a). A similar behavior occurs for Neptune (Fig. 4b).

It is worth emphasizing that, for the initial conditions along the energy level *b*, the spectral map does not show any changes around the fixed point of Mode I of motion. There is a simple (qualitative) physical explanation for the unstable nature of trajectories around the Mode II, at variance with the stable configuration of Mode I. In Mode I, the lines of apses of the planets are always aligned at the same direction, either at $\sigma_1 = 0$ and $\sigma_2 = 0$ (MI+) or at $\sigma_1 = \pi$ and $\sigma_2 = \pi$ (MI-). In Mode II, the planetary lines of apses are always anti-aligned, either at $\sigma_1 = 0$ and $\sigma_2 = \pi$ (MII+) or at $\sigma_1 = \pi$ and $\sigma_2 = 0$ (MII-). These four possible geometrical configurations of the planets are shown in Fig. 5, where the initial positions of the planets are indicated by 1 and the intermediate positions by 2. Figure 5 shows that, at conjunctions, the very close approach between the two planets occurs at MII-. In the near-resonance domain, where the secular perturbations dominate the dynamics of the system, this configuration remain stable (at least for the mass ratio under study). However, under growing resonant perturbations, trajectories from the neighborhood of MII- become unstable. In Mode I of motion, at the conjunctions, Uranus is at perihelion and Neptune at aphelion of their orbits. This is a stable resonant configuration of the system. However, as we will see in Section 4.6, the stability of Mode I on the sections of the kind $\underline{b}$ is guaranteed up to $H = +1.51 \times 10^{-9}$ only.

4.3 Regime III

For energies larger than $H = +1.33622 \times 10^{-9}$ (level *b*), the system enters into the resonance zone, and the main features of the 2/1 resonance appear. Let us consider, now, the levels *c, d, e, f* from Table I; the corresponding sections are shown in Fig. 6. A new resonant regime of motion appears besides the retrograde circulations (C_R) of Modes I and II in Fig. 6a. In this regime, designated as Regime III of motion, σ_1 librates around 0, while σ_2 and $\Delta\varpi$ librate around π.

In the spectral map (Fig. 6a bottom), the resonant Regime III appears clearly separated from the secular regime of motion by a true separatrix, denoted by S1 on the sections. The vertical broad lines seen in the spectral map correspond to the chaotic separatrix trajectories. Note that the curves S1 on the sections do not show any visible indication of chaotic motion. In the region between S1 and the frontier of Mode I, σ_2 and $\Delta\varpi$ alternate between libration and circulation, while σ_1 remains librating around zero. We note in Fig. 6a bottom that circulation orbits of Mode II are still present, and Mode I is entirely preserved under the resonant perturbations.

For growing energy, the domain of Regime III increases, as we can see in the sequence of the panels in Fig. 6a-6c. The fixed point of this regime of motion gradually moves toward the left-hand edge on Uranus section, while, on the Neptune section, it moves toward the origin (Fig. 6d). Mode II remains outside the separatrix S1 occupying a decreasing zone on the sections and spectra maps; Mode I is always present.

One periodic solution obtained at Regime III of motion is shown in Figs. 7a,b and illustrates the coupled libration of the critical angles σ_1 and σ_2. The secular angle $\Delta\varpi$ represented by the coupled libration of the critical angles, librates around π.

4.4 Regime IV and changes in Regime III

A new regime of motion appears at the slightly larger energy g from Table I. As we can see in Fig. 8a, this mode, designated as Regime IV, appears just inside the domain of Regime III. A new separatrix associated with this regime is plotted on the sections by the curves S2. The chaotic character of motion near S2 is confirmed by the spectral map: The monotonic evolution of the frequencies inside Regime III is now broken up and discontinuities appear. The frequency of the secular angle $\Delta\varpi$ tends to zero near S2: this is a feature of the infinite-period separatrix of the secular resonance. In the regime R IV, the critical angles σ_1 and σ_2 continue to librate around 0 and π, respectively. The difference between regimes III and IV is in the motion of the angle $\Delta\varpi$: now it librates around π in a direction opposite to that of Regime III. This change in the direction of motion of the secular angle $\Delta\varpi$ is an other feature of the secular resonance. Therefore, we conclude that Regime III is the secular resonance located inside the 2/1 mean-motion resonance.

As the energy is increased, Regime III of motion suffers some changes: σ_1 continues to librate around 0, while σ_2 changes its libration around π to one around 0. We have detected this transition at $H \approx +1.497 \times 10^{-9}$ and present the corresponding planetary trajectories in Fig. 7c,d. It should be emphasized that the passage of the center of libration of σ_2 through the origin (consequently, the center of libration of σ_1 reaches the energy edge on Uranus section) is merely kinematical, and a new separatrix does not appear on the sections. Due to this fact, we maintain the same name for this type of motion.

4.5 Splitting of Regime III and enlargement of Regime IV

Fig. 8b shows the surfaces of sections constructed along the energy level h from Table I. The fixed point of Regime III of motion is now in the right-hand side on Neptune section, passing through the origin of the section from π to 0. On Uranus section, the center of Regime III is squeezed against the energy border. Since it leaves the x axis, the periodic orbit of the Regime III cannot be seen in the spectral map constructed with the condition $\sin\Delta\varpi = 0$. We note that Regime III arises with anti-aligned orbits and evolves continually to have aligned orbits, what can be seen in the sequence of the panels shown in Fig. 7. (Similar behavior of Regime III was observed in the construction of the sections b).

We end this section describing the other regimes present in Fig. 8b. The Regime IV increases its domain and the separatrix S2 is now located near the origin of Uranus section and the spectral map. The secular Mode I is still present on the sections and spectral map in spite of the resonant perturbations.

4.6 Study of the four sections

The analysis of the main features of the dynamics of the resonant system present above was done over the surfaces of section of the kind a. In this section, we investigate the sections constructed for the four roots a, b, c and d of eq. (11), along the energy level i (Fig. 1). They are shown in Fig. 9a,b. The spectral maps corresponding to Uranus sections a and b are also shown in Fig. 9a.

The Uranus and Neptune sections a and b constructed at the energy ($H \approx +1.51 \times 10^{-9}$) are plotted in Fig. 9a,b top. Regimes III and IV of resonant motion are present on all sections. It should be emphasized that the corresponding fixed points on the sections a and b are obtained with different initial conditions and, consequently, are not equivalent.

On the section a, Mode I of secular motion occupies a large domain of stable motion (Fig. 9a,b top left). At variance, on the section b, its domain, delimited from the regions of resonant motion by the separatrix S1, is vanishing (Fig. 9a,b top right).

We finish this section analyzing the surfaces of sections c and d shown in Fig. 9a,b bottom. As pointed in Section 3, some information would be lost if these sections have been used in the study of the resonant dynamics of the system. Indeed, the information on Regime IV is not present in the figures, which do not show the fixed point associated to this regime.

4.7 Regime V

The formation of a new regime of motion can be seen at slightly larger values of energy in Fig. 10. This figure shows the sequence of Uranus sections b . The new regime, designated as Regime V, replaces the extinct Mode I of motion on the sections b. Its evolution with the increasing energy can be observed on the sections shown at an enlarged scale in Fig. 10. The complex structure of the phase space is characterized by the presence of secondary resonances and regions of chaotic motion. At $H \approx +1.517 \times 10^{-9}$, a new structure appears (Fig. 10g), increases its domain up to $H \approx +1.526 \times 10^{-9}$ (Fig. 10i) and disappears at $H \approx +1.5265 \times 10^{-9}$ (Fig. 10l). In Regime V of motion, σ_1 and $\Delta\varpi$ show retrograde and direct circulations, respectively, while σ_2 librates around π. The periodic motions of Uranus (a) and Neptune (b) in this regime are shown in Fig. 11.

The domain of Regime V is located in the proximity of the origin on the Uranus section a and the energy boundary on Neptune section a (see details in the right-hand side in Fig. 12). It is enclosed by chaotic orbits of the separatrices S1 and S2. The spectral maps in Fig. 12 bottom reveal the highly nonharmonic nature of the orbits in Regime V of motion.

For energies larger than $\mathcal{H} = +\infty.\bigtriangledown\in\ni \times \infty\prime^{-\exists}$ (level j from Table I), Regimes III and V disappear, and Mode I and Regime IV are only remaining on the sections a. As the energy is increased, the domains of these regimes gradually decrease and disappear at the energy of the equilibrium point PII$^+$. Figure 13a,b shows two examples of the surfaces of section obtained along the levels k ($H = +1.55 \times 10^{-9}$) and l ($H = +1.90 \times 10^{-9}$). This later is located very close to the equilibrium point PII$^+$. The corresponding spectral maps reveal the presence of the two fundamental frequencies and their harmonics. On the sections b, only Regime IV is remaining at energy $H \sim +1.5265 \times 10^{-9}$ (for example, see Fig. 10l), until to disappear at the maximal energy $H \approx +1.9171 \times 10^{-9}$.

5 The parameter plane

In Section 4, we have presented the results of the investigation of the dynamics of Uranus-Neptune system obtained with the value of δ fixed at 0.0012. The aim of this section is to explore the dynamics of the systems for different values of δ.

As pointed in Section 3, the topology of the phase space given by the Hamiltonian (11) is characterized by three zero-gradient points: C, PII$^-$ and PII$^+$. The location of these points on the representative plane (e_1, e_2) depends on the chosen value of δ through $H = f(x_1(e_1), x_2(e_2); \delta)$ and $y_1 = y_2 = 0$. The energy levels corresponding to these points delimit the main domains of motion: the resonance zone, where $H(\text{PII}^-) \leq H \leq H(\text{PII}^+)$, and the near-resonance zone, where $H_{\min} \leq H < H(\text{PII}^-)$. Therefore, in order to investigate the dependence of the 2/1 resonance dynamics on δ, we need to know the position of three zero-gradient points on the (e_1, e_2)–plane as a function of δ.

The coordinates (e_1, e_2) of the zero-gradient points of H as a function of δ are obtained by means of numerical integration of eqs. (12). Fig. 14 shows the coordinates (e_1, e_2) obtained for the points C, PII$^-$ and PII$^+$. The x–axis shows the values of δ and the y–axis shows the value of eccentricities of the points. It should be noted that the points C and PII$^-$ exist only for $\delta \geq 0.0003$. For $\delta \leq 0.0003$, there is only the equilibrium point PII$^+$ of zero gradient on the plane of initial conditions. In this case, the system is far away from the 2/1 resonance, and its dynamics is dominated by secular perturbations. These results are in good agreement with the results of the study of families of periodic orbits of the planetary type presented by Hadjidemetriou and Psychoyos (2003).

Once the eccentricities of the equilibrium points C, PII$^-$ and PII$^+$ are known, we are able to calculate the energy of these points as a function of δ. Here, we introduce the plane defined by two parameters of the problem under study, δ and H. In order to better visualize the results, we use a normalized value of the energy given by $\Delta E = H - H^{II}_{\text{sec}}$, where H^{II}_{sec} is the energy of the point PII$^-$ obtained from the secular Hamiltonian (see MF2001a for details; see also the brief discussion in Section 4.1).

The main features of the dynamics of the 2/1 resonance are summarized on the parameter plane (δ,ΔE) shown in Fig. 15. The region above the curve PII$^+$ is a forbidden region, where no real solutions of the Hamiltonian (11) exist. The 2/1 resonance zone is located between the curves PII$^+$ and PII$^-$. In this region, there exist initial conditions leading to several regimes of motion described in the previous sections. Since the limits of the regimes are located between the curves PII$^+$ and PII$^-$, we can say that they *may* exist for $\delta \geq 0.0003$ values. (Note that we cannot guarantee that *all* regimes of motion detected in resonance zone for $\delta = 0.0012$ exist for any δ value).

The region between the curves C and PII$^-$ is the near-resonance domain, where both retrograde (C_R) and direct (C_D) circulations of the critical angles σ_1 and σ_2 are possible. The full circle inside the near-resonance region indicates the actual position of the Uranus-Neptune system, whose dynamics is dominated by secular interactions. Below the curve C, only retrograde circulation (C_R) of the critical angles exists.

We complete Fig. 15 by plotting the energies of the separatrices of two single-term resonances, obtained by removing artificially the coupling terms from the Hamiltonian (11). In this way, we obtain two Andoyer Hamiltonians given by

$$\begin{aligned} H_1 &= B(x_1^2+y_1^2)^2 + \frac{\delta}{2}(x_1^2+y_1^2) + Fx_1 \\ H_2 &= B(x_2^2+y_2^2)^2 + \frac{1}{2}[\delta - 2(C-D)](x_2^2+y_2^2) + Ix_2. \end{aligned} \tag{13}$$

The separatrices given by H_1 and H_2 are indicated in Fig. 15 by SPX1 and SPX2, respectively.

6 Conclusions and Discussion

We have performed several numerical experiments with the planar model that represents the 2/1 mean-motion resonance in planetary systems. The model was applied to the system Sun-Uranus-Neptune, which is actually close to the 2/1 resonance. The dynamics of this system was studied by means of surfaces of section and spectral analysis of the solutions obtained over a wide range of initial conditions. The main conclusions are summarized in the following.

Far away from the 2/1 resonance, the critical angles σ_1 and σ_2 are in a retrograde circulation (the secular regime C_R), and the dynamics of the systems is dominated by secular interactions. The secular angle $\Delta\varpi$ oscillates around 0 (secular Mode I) or π (secular Mode II), depending on the initial condition. When the system is outside one of the secular modes, $\Delta\varpi$ is in a retrograde circulation. When the 2/1 resonance is approached, the system enters into the near-resonance region, where the direct circulation of both σ_1 and σ_2 may occur (the secular regime C_D).

In the region of transition from near-resonance to resonance, the behavior of the system is chaotic. In the transition regime of motion, the critical angles alternate their circulation regime between direct and retrograde circulations.

In the domain of the 2/1 resonance, there are three different regimes of motion:

Regime III: the secular resonance inside the 2/1 mean-motion resonance. In this regime, σ_1 librates around 0, while σ_2 ($\Delta\varpi$) librates around either π or 0. The domain of the secular resonance is separated by the chaotic layers S1 and S2 from the near-resonance and resonance regions, respectively.

Regime IV: the dominating 2/1 resonance regime of motion, when σ_1 librates around 0. The angles σ_2 and $\Delta\varpi$ librate or circulates around π (the difference is merely kinematical). In this regime, the motion of the system can be approximated by the first-order e_1 single-term resonance given by the Hamiltonian H_1 (eq. 13).

Regime V: the weak regime that can be, in first order, approximated by the single-term resonance given by the Hamiltonian H_2 (eq. 13). The angles σ_1 and $\Delta\varpi$ circulate in retrograde and direct directions, respectively, while σ_2 librates around π.

Some insight on the size of the domains of the different regimes of motion can be gained by constructing the dynamical map of the representative plane of initial conditions (e_1, e_2). It is shown in Fig. 16. The gray-scale code is related to the degrees of stochasticity of the initial conditions: white corresponds to regular orbits, while darker gray levels indicate the increasingly chaotic motion. The construction of the map was based on the calculation of the spectral number N, defined as the number of significant (more than 10% of the larger peak) spectral peaks in the oscillation of the variables x_i, $i = 1, 2$ (for further details about the map construction see MF2001a, Michtchenko and Ferraz-Mello 2000).

The regions in white ($N = 1$) correspond to the periodic orbits associated with the main regimes of motion (some of these are indicated by symbols - see legend in Fig. 16). The plane is dominated by the regions in light gray, which correspond to regular motion of the system (quasi-periodic solutions). The dark regions correspond to highly nonharmonic and chaotic motion associated with the solutions close to the separatrices S1 and S2.

For $\delta = 0.0012$, the phase space is dominated by the secular regime and the resonant regime RIV of motion. The domains of the regimes RIII and RV are confined to the very narrow zones located deeply inside dark regions of chaotic motion. The domains of Regimes III and V are not robust, and they could not survive in a more complex model.

The described properties of the 2/1 resonance were obtained for the planet mass ratio $\frac{m_1}{m_2} \approx 0.847$, with $m_2 > m_1$. We have also performed numerical experiments with different mass ratios: three of them with the mass of the inner planet larger than the outer one ($m_1 > m_2$) (mass ratio $1.18, 1.77, 8.77$), and one with $m_1 = m_2$. The main features of the 2/1 resonant dynamics described in this paper, such as the secular regime, Regimes III, IV and V of motion were observed in all cases. However, to get a better knowledge on the sensitivity of the 2/1 resonant dynamics upon the different mass configurations, a complete study would be necessary.

Appendix

This appendix gives the expressions for the coefficients of the Hamiltonian (11). They are functions of the semi-major axes ratio $\alpha = \frac{a_1}{a_2}$, and the masses m_0, m_1, m_2 of the central star, inner and outer planets, respectively.

The coefficients a, b, c, d, e, f, g, h in eq. (6) are functions of α only. Denoting with $D_\alpha = \frac{d}{d\alpha}$, $D_\alpha^2 = \frac{d^2}{d\alpha^2}$ the derivatives of the Laplace coefficients $b_s^i(\alpha)$, we have the following expressions:

$$\begin{aligned}
a &= \frac{1}{2} b_{1/2}^{(0)} \\
b &= \frac{1}{2}(2\alpha D_\alpha + \alpha^2 D_\alpha^2) b_{1/2}^{(0)} = \frac{1}{2}\alpha b_{3/2}^{(1)} \\
c &= (2 - 2\alpha D_\alpha - \alpha^2 D_\alpha^2) b_{1/2}^{(1)} = -\alpha b_{3/2}^{(2)} \\
d &= -[2(1+r) + \alpha D_\alpha] b_{1/2}^{(1+r)} \\
e &= (2r + 1 + \alpha D_\alpha) b_{1/2}^{(r)} + \vartheta \\
f &= \left[16(1+r)^2 - 10(1+r) + (8r-6)\alpha D_\alpha + \alpha^2 D_\alpha^2\right] b_{1/2}^{2(1+r)} \\
g &= \left[16r^2 + 18r + (8r+6)\alpha D_\alpha + \alpha^2 D_\alpha^2 + 4\right] b_{1/2}^{(2r)} \\
h &= -\left[4(2r+1)^2 + 2(2r+1) + (8r+6)\alpha D_\alpha + \alpha^2 D_\alpha^2\right] b_{1/2}^{(2r+1)},
\end{aligned} \tag{14}$$

where $r = 1$. The term ϑ which appears in the coefficient e comes from the indirect part of the disturbing function and is present only in the case of first-order resonances. It is given by:

$$\vartheta = -\sqrt{\frac{a_2}{a_1}} \frac{m_0}{\sqrt{(m_1 + m_0)(m_2 + m_0)}}. \tag{15}$$

The coefficients A, B, C, D, E, F, R, S, T in eq. (10) appear in the expansion of the Hamiltonian (6) in I_i, $i = 1, 2$, and are given by:

$$\begin{aligned}
A &= \frac{1}{2}Gm_0\left[-\frac{k_1 r}{J_1^3}+\frac{k_2(r+1)}{J_2^3}\right], \\
B &= -\frac{3}{8}Gm_0\left[\frac{k_1 r^2}{J_1^4}+\frac{k_2(r+1)^2}{J_2^4}\right], \\
C &= \frac{1}{2}k_{12}\left\{\frac{-b}{J_1 J_2^2}+\frac{2(r+1)a}{J_2^3}+\frac{2}{J_2^2}\frac{da}{d\alpha}\frac{\beta_2^2\mu_2}{\beta_1^2\mu_1}\left[\frac{J_1 r}{J_2^2}+\frac{J_1^2(r+1)}{J_2^3}\right]\right\}, \\
D &= \frac{1}{2}k_{12}\left\{\frac{1}{J_2^3}\left[-b+2(r+1)a\right]+\frac{2}{J_2^2}\frac{da}{d\alpha}\frac{\beta_2^2\mu_2}{\beta_1^2\mu_1}\left[\frac{J_1 r}{J_2^2}+\frac{J_1^2(r+1)}{J_2^3}\right]\right\}, \\
E &= \frac{-k_{12}c}{4J_2^2\sqrt{J_1 J_2}}, F=\frac{-k_{12}d}{2J_2^2\sqrt{J_1}}, I=\frac{-k_{12}h}{2J_2^2\sqrt{J_2}}, \\
R &= \frac{-k_{12}f}{8J_1 J_2^2}, S=\frac{-k_{12}g}{8J_2^3}, \\
T &= \frac{-k_{12}h}{4J_2^2\sqrt{J_1 J_2}},
\end{aligned} \tag{16}$$

with $k_1 = \mu_1\beta_1^2 m_1$, $k_2 = \mu_2\beta_2^2 m_2$, $k_{12} = Gm_1 m_2\mu_2\beta_2^2$.

The last terms in the expressions for the coefficients C and D come from the expansion of the quantity $\frac{a}{a_2}$ given in eq. (7) (Section 2). This expansion must be done since this term is not multiplied by any eccentricity, and these corrections are of order $O(I_i)$.

Table II: Numerical values of the semi-major axes defining the exact resonances and constants J_{i0}

	a (AU)	J_{i0}
Uranus	19.0737	1.1981×10^{-3}
Neptune	30.2778	1.7809×10^{-3}

Table III: Numerical values of coefficients of the Hamiltonian

Coefficient	Numerical Value
B	-55.37
C	$+5.8250\times10^{-6}$
D	$+6.4460\times10^{-6}$
E	$+1.1557\times10^{-6}$
F	$+1.0086\times10^{-7}$
I	-7.3549×10^{-8}
R	-4.1779×10^{-9}
S	-1.0003×10^{-8}
T	$+1.7759\times10^{-8}$

Acknowledgements

Nelson Callegari Jr. thanks Fapesp for financial support (proc. 98/13593-8), F. Roig, T. Yokoyama for discussions.

References

[1] Beaugé, C: 1994. "Asymmetric Librations in Exterior Resonances". *Celest. Mech. Dyn. Astr.*, **60**, 225.

[2] Beaugé, C., S. Ferraz-Mello, T. A. Michtchenko: 2003. "Extrasolar Planets in Mean-Motion Resonance: Apses Alignment and Asymmetric Stationary Solutions". *Astroph. J.*, **593**, 1124.

[3] Callegari Jr., N.: 2003. "Ressonâncias 2:1 e 3:2 em sistemas planetários". *Dr. Thesis, Univ. Sao Paulo, SP.*

[4] Everhart, E.: 1985. "An efficient integrator that uses Gauss-Radau spacings". *IAU Coloquium*, **83**, 185.

[5] Ferraz-Mello, S.: 2002. "Tidal Acceleration, Rotation and Apses Alignment in Resonant Extra-Solar Planetary Systems". *Bull. Amer. Astron. Soc.*, **3**, 892.

[6] Ferraz-Mello, S., C. Beaugé, T. A. Michtchenko: 2003. "Evolution of Migrating Planet Pairs in Resonance". *Celest. Mech. Dyn. Astr.*, **87**, 99.

[7] Ferraz-Mello, S., T. A. Michtchenko, C. Beaugé: 2004. "Regular Motions in Extra-Solar Planetary Systems", to be published in "Chaotic Worlds: From Order to Disorder in Gravitational N-Body Systems" (B.A,Steves, ed.), Kluwer Acad. Publ., preprint astro-ph/0402335.

[8] Gladman, B.: 1993. "Dynamics of systems of two close planets". *Icarus*, **106**, 247.

[9] Hadjidemetriou, J. D.: 1985. "The stability of resonant orbits in planetary systems". In S. Ferraz-Mello and W. Sessin, editors, *Resonances in the Motion of the Planets, Satellites and Asteroids*, IAG/USP, Sao Paulo.

[10] Hadjidemetriou, J. D., D. Psychoyos: 2003. "Dynamics of extrasolar planetary systems: 2/1 resonant motion". In G. Coutopoulos and N. Voglis, editors, *Lectures Notes in Physics: Galaxies and Chaos*, 412-432. Springer-Verlag.

[11] Hori, G.: 1985. "Mutual perturbations of 1:1 commensurable small bodies with the use of the canonical relative coordinates. Part I". In S. Ferraz-Mello and W. Sessin, editors, *Resonances in the Motion of the Planets, Satellites and Asteroids*, IAG/USP, Sao Paulo.

[12] Israelian, G., N. Santos, M. Mayor, and R. Rebolo: 2001. "Evidence for planet engulfment by the star HD82943". *Nature*, **411**, 163.

[13] Kinoshita, H., H. Nakai: 2001. "Stability of the GJ 876 Planetary system". *Publ. Astron. Soc. Japan*, **53**, L25.

[14] Laskar, J.: 1989. "A numerical experiment on the chaotic behavior of the solar system". *Nature*, **338**, 237.

[15] Laskar, J., P. Robutel: 1995. "Stability of the planetary three-body problem I: Expansion of the Planetary Hamiltonian". *Celest. Mech. Dyn. Astr.*, **62**, 193.

[16] Le Verrier, U. J.: 1855. "Recherches Astronomiques. Ch. IV: Developpement de la fonction qui sert de base au calcul des perturbations des mouvements des planètes". *Ann. Obs. Paris*, tome 1, 258.

[17] Lecar, M., F. A. Franklin, M. J. Holman, N. J. Murray: 2001. "Chaos in the Solar System". *Annual Review of Astron. and Astrophys.*, **39**, 581.

[18] Lee, M. H., S. J. Peale: 2002. "Dynamics and origin of the 2:1 resonances of the GJ 876 planets". *Astroph. J.*, **567**, 596.

[19] Marcy, G. M., R. P. Butler, D. Fisher, S. S. Vogt, J. J. Lissauer, E. J. Rivera: 2001. "A pair of resonant planets orbiting GJ 876". *Astroph. J.*, **556**, 296.

[20] Malhotra, R.: 1992. "Resonant orbital evolution in the putative planetary system of PSR1257 +12". *Nature*, **356**, 583.

[21] Malhotra, R.: 1998. "Orbital Resonances and Chaos in the Solar System". In D. Lazzaro et al. editors, *Solar System Formation and Evolution ASP Conference Series*, Brazil, **149**, 37.

[22] Malhotra, R.: 2002. "A Dynamical Mechanism for Establishing Apsidal Resonance". *Astroph. J.*, **575**, L33.

[23] Michtchenko, T. A., S. Ferraz-Mello: 2000. "Periodic Solutions of the Planetary 5:2 Resonance Three-Body Problem". In R. Dvorak and J. Henrard editors, *New Developments in the Dynamics of Planetary Systems*, 325.

[24] Michtchenko, T. A., S. Ferraz-Mello: 2001a. "Modeling the 5:2 Mean-motion Resonance in the Jupiter-Saturn Planetary System". *Icarus*, **149**, 357.

[25] Michtchenko, T. A., S. Ferraz-Mello: 2001b. "Resonant Structure of the Solar System in the Neighborhood of the Planets". *Astron. J.*, **122**, 474.

[26] Michtchenko, T. A., R. Malhotra: 2004. "Secular Dynamics of the Three-Body Problem: Application to the υ Andromedae Planetary System". *Icarus*, (in press).

[27] Milani, A., A. M. Nobili: 1984. "Resonance locking between Jupiter and Uranus". *Nature*, **310**, 753.

[28] Nobili, A. M., A. Milani, M. Carpino: 1989. "Fundamental frequencies and small divisors in the orbits of the outer planets". *Astron. and Astrophys.*, **210**, 313.

[29] Murray, N., M. Holman: 1999. "The Origin of Chaos in the Outer Solar System". *Science*, **283**, 1877.

[30] Pauwels, T.: 1983. "Secular orbit-orbit resonance between two satellites with non-zero masses". *Celest. Mech.*, **30**, 229.

[31] Poincaré, H.: 1897. "Une forme nouvelle des équations du problème des trois corps". *Bull. Astron.*, **14**, 53.

[32] Rasio, F. A., P. D. Nicholson, S. L Shapiro, S. A. Teukolsky: 1992. "An observational test for the existence of a planetary system orbiting PSR 1257+12". *Nature*, **355**, 325.

[33] Sessin, W., S. Ferraz-Mello: 1984. "Motion of two planets with periods commensurable in the ratio 2:1/ Solutions of the Hori auxiliary system". *Celestial Mechanics*, **32**, 307.

[34] Sussman, G. J., J. Wisdom: 1988. "Numerical evidence that the motion of Pluto is chaotic". *Science*, **241**, 433.

[35] Tittemore, W., J. Wisdom: 1988. "Tidal evolution of the Uranian satellites I. Passage of Ariel and Umbriel through the 5:3 Mean-Motion Commensurability". *Icarus*, **74**, 172.

[36] Varadi, F., M. Ghil, W. M. Kaula: 1999. "Jupiter, Saturn, and the Edge of Chaos". *Icarus*, **139**, 294.

[37] Wolszczan, A., D. A. Frail: 1992. "A planetary system around the millisecond pulsar PSR 1257+12". *Nature*, **355**, 145.

FIGURES

Fig1. Energy level curves of the Hamiltonian given by eq. (11) on the plane of initial conditions for the 2/1 resonance of the Uranus-Neptune system. The initial values of $y_i = e_i \sin \sigma_i$ are fixed at zero and $\delta = 0.0012$. The points PII$^-$, PII$^+$ and C are points of zero gradient of the Hamiltonian (11). The thick curves are locations of the conditions $\dot{\sigma}_1 = 0$ and $\dot{\sigma}_2 = 0$.

Fig2. Top: Surfaces of section of Neptune. Middle: surfaces of section of Uranus. The thick curves are the boundaries of the energy manifold. Bottom: spectral maps corresponding to the solutions shown on the Uranus sections. $\delta = 0.0012$. The main regimes of motion are indicated at the bottom of the panels. a) Energy level *a* from Table I and Fig. 1. b) Energy level *b*.

Fig3. The enlarged domain of initial conditions around the equilibrium point PII$^-$ shown in Fig. 1.

Fig4. a) Periodic orbits of Uranus in the neighborhood of the equilibrium point PII$^-$. The arrows show the direction of motion of the critical angle σ_1, and the points show the initial positions of the planets. Chaotic behavior around the center of Mode II is explained by a transition between the direct and retrograde motions. b) The same for Neptune, except the critical angle σ_2.

Fig5. Periodic orbits of the Modes I and II. In Mode I the lines of the planetary apses are aligned. In Mode II they are anti-aligned. The number 1 indicates the initial configuration of the planets; 2 indicates the planetary configuration after one revolution of the inner planet. After one revolution of the outer planet, they are both back to 1.

Fig6ab. The same as in Fig. 2. a) Energy level *c* from Table I. b) Energy level *d*. c) Energy level *e*. d) Energy level *f*.

Fig6cd. Fig. 6: Continued.

Fig7. Examples of the resonant periodic orbits in Regime III. Left column: the periodic orbits of Uranus. Right column: the periodic orbits of Neptune. Points indicate initial planet positions, and arrows show the direction of motion. a,b) coupled libration of the critical angles (the energy level *c*). c,d) Libration of σ_1 and circulation of σ_2, for energy level $H = +1.497 \times 10^{-9}$. e,f) coupled libration of the critical angles around 0 (energy level *i*).

Fig8. The same as in Fig. 2. a) Energy level *g* from Table I. b) Energy level *h*.

Fig9. a) Uranus sections and spectral maps over energy level *i*. Top: surfaces of section of the kind a (left) and b (right). Middle: spectral maps corresponding to the sections a (left) and b (right). Bottom: Surfaces of section of the kind c (left) and d (right). b) Neptune surfaces of section corresponding to sections given in figure a). Top: sections a (left) and b (right). Bottom: sections c (left) and d (right).

Fig9b. Figure 9: Continued.

Fig10. The enlarged domains of Regime V of motion. At $H \approx +1.511 \times 10^{-9}$ (b), a complex dynamical structure arises in the phase space, which survives up to $H \approx +1.514 \times 10^{-9}$ (10e). The nature of this structure was not studied in detail, but it probably involves secondary resonances. For $H \approx +1.517 \times 10^{-9}$ a new robust mode of motion appears, the Regime V.

Fig11. Example of the resonant motion in Regime V: (a) periodic orbit of Uranus, (b) periodic orbit of Neptune. Points show initial positions of the planets, and arrows show the direction of motion. In figure a, numbers 1-4 represent four steps of simulation, in which σ_1 begins with retrograde circulation (1), evolves in a direct circulation (2,3), and returns to retrograde circulation (4). The energy corresponds to level *j* from Table I.

Fig12. a) Surfaces of section of Neptune. b) Surfaces of section of Uranus. c) Spectral maps corresponding to the solutions shown on the Uranus section. The main regimes of motion are indicated on the sections. Energy level *j* from Table I. Panels on the right-hand side are the enlarged regions of the figures a, b and c.

Fig13. The same as in Fig. 2. a) Energy level *k* from Table I. b) Energy level *l*. Scale and axes are the same in both figures.

Fig14. Coordinates of the three zero-gradient points C, PII$^-$ and PII$^+$ of the Hamiltonian (11) as a function of δ. The condition $e_i < 0$ means that $\sigma_i = \pi$ and $e_i > 0$ means that $\sigma_i = 0, i = 1, 2$.

The coordinates of the points C, PII^- and PII^+ shown in Fig. 1, are indicated by vertical line, for $\delta = 0.0012$.

Fig15. The (δ,ΔE) parameter plane. The resonance zone is located between curves PII^+ and PII^-, and the near-resonance zone between PII^- and C. C_R: retrograde circulation, C_D: direct circulation. Full circle represents the actual position of the Uranus-Neptune system.

Fig16. The dynamical map of the representative plane of initial conditions, for $\delta = 0.0012$. The labels represent the main regimes of motion. Full symbols represent some initial conditions of the periodic orbits obtained from sections b, while open symbols represent the same orbits obtained from sections a (Callegari 2003). Circles: R III, squares: R IV, stars: R V. The location of the points PII^+, PII^- and C shown in Fig. 1 is also indicated.

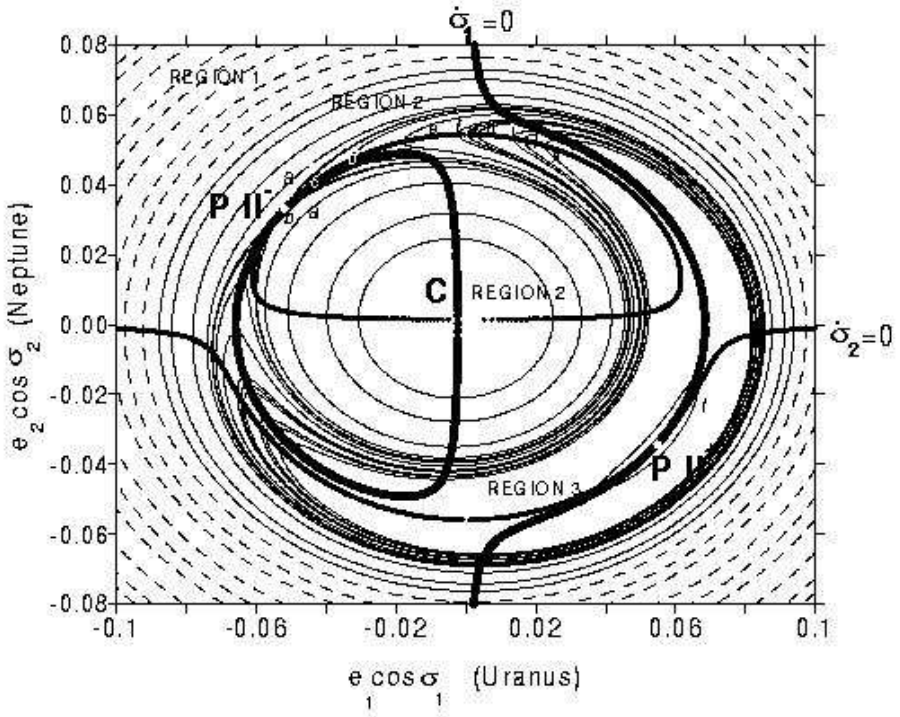

Figure 1: Energy level curves of the Hamiltonian given by eq. (11) on the plane of initial conditions for the 2/1 resonance of the Uranus-Neptune system. The initial values of $y_i = e_i \sin \sigma_i$ are fixed at zero and $\delta = 0.0012$. The points PII^-, PII^+ and C are points of zero gradient of the Hamiltonian (11). The thick curves are locations of the conditions $\dot{\sigma}_1 = 0$ and $\dot{\sigma}_2 = 0$.

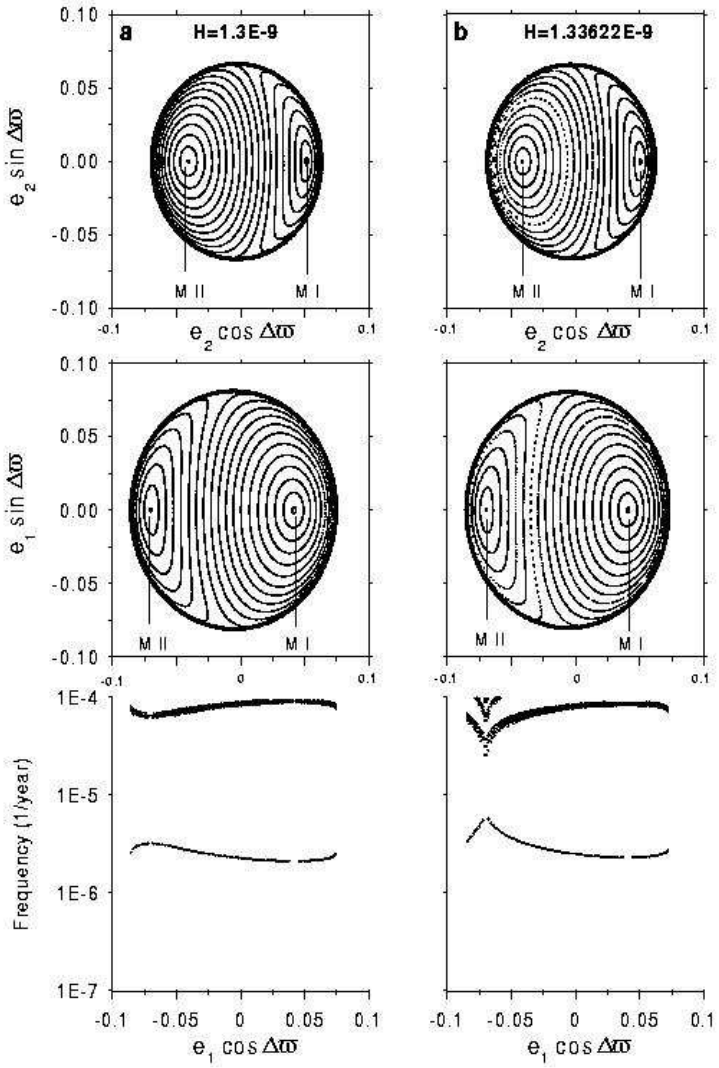

Figure 2: Top: Surfaces of section of Neptune. Middle: surfaces of section of Uranus. The thick curves are the boundaries of the energy manifold. Bottom: spectral maps corresponding to the solutions shown on the Uranus sections. $\delta = 0.0012$. The main regimes of motion are indicated at the bottom of the panels. a) Energy level *a* from Table I and Fig. 1. b) Energy level *b*.

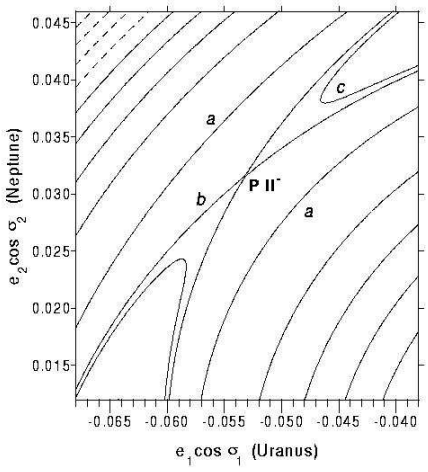

Figure 3: The enlarged domain of initial conditions around the equilibrium point PII^{-} shown in Fig. 1.

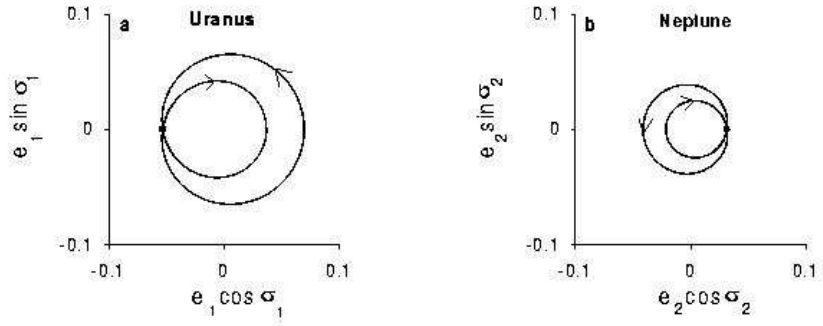

Figure 4: a) Periodic orbits of Uranus in the neighborhood of the equilibrium point PII^{-}. The arrows show the direction of motion of the critical angle σ_1, and the points show the initial positions of the planets. Chaotic behavior around the center of Mode II is explained by a transition between the direct and retrograde motions. b) The same for Neptune, except the critical angle σ_2.

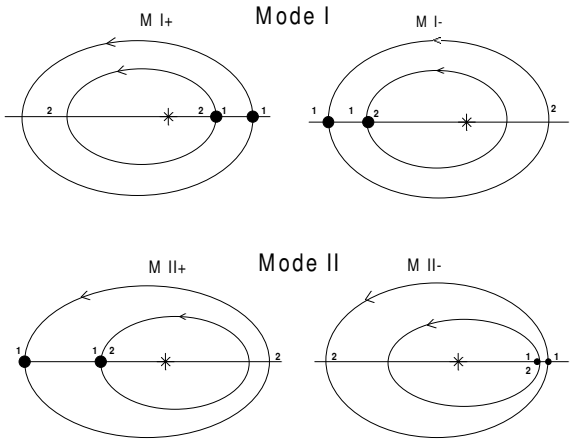

Figure 5: Periodic orbits of the Modes I and II. In Mode I the lines of the planetary apses are aligned. In Mode II they are anti-aligned. The number 1 indicates the initial configuration of the planets; 2 indicates the planetary configuration after one revolution of the inner planet. After one revolution of the outer planet, they are both back to 1.

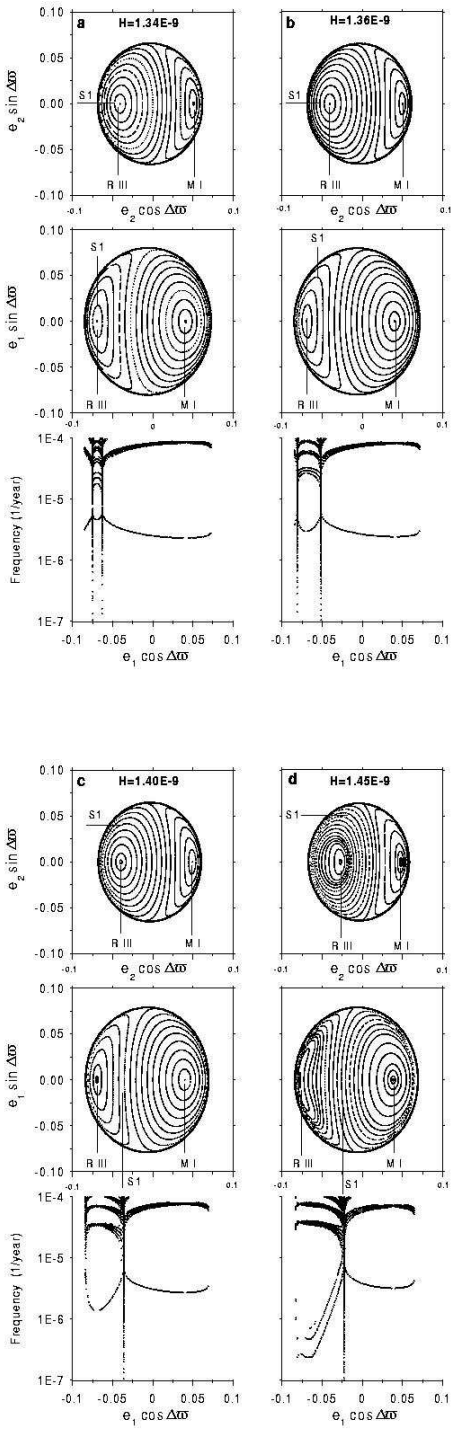

Figure 6: The same as in Fig. 2. a) Energy level *c* from Table I. b) Energy level *d*. c) Energy level *e*. d) Energy level *f*.

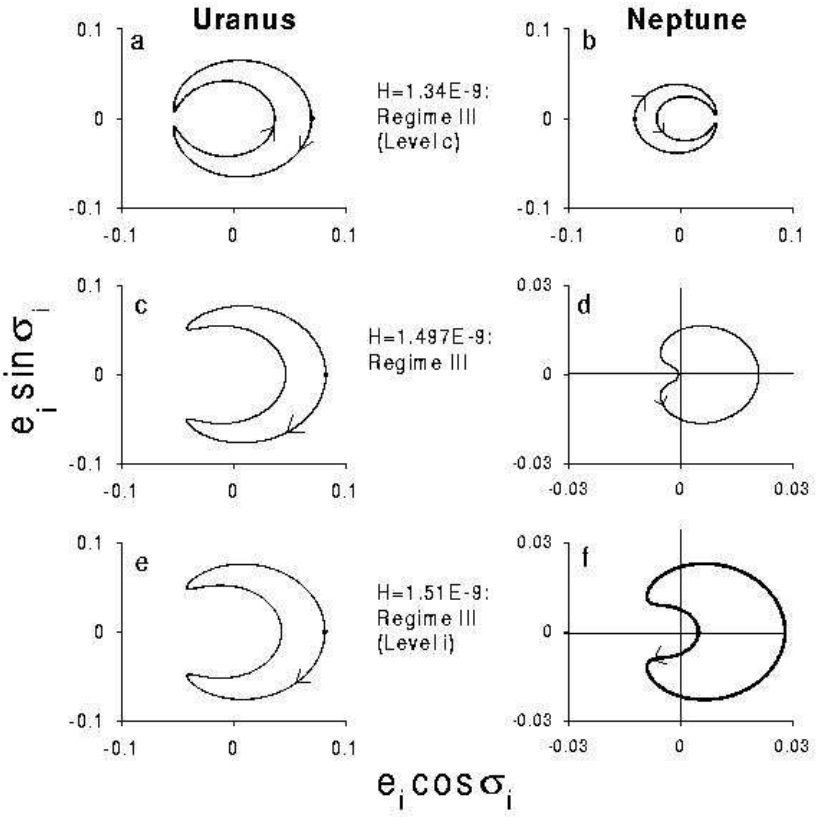

Figure 7: Examples of the resonant periodic orbits in Regime III. Left column: the periodic orbits of Uranus. Right column: the periodic orbits of Neptune. Points indicate initial planet positions, and arrows show the direction of motion. a,b) coupled libration of the critical angles (the energy level c). c,d) Libration of σ_1 and circulation of σ_2, for energy level $H = +1.497 \times 10^{-9}$. e,f) coupled libration of the critical angles around 0 (energy level i).

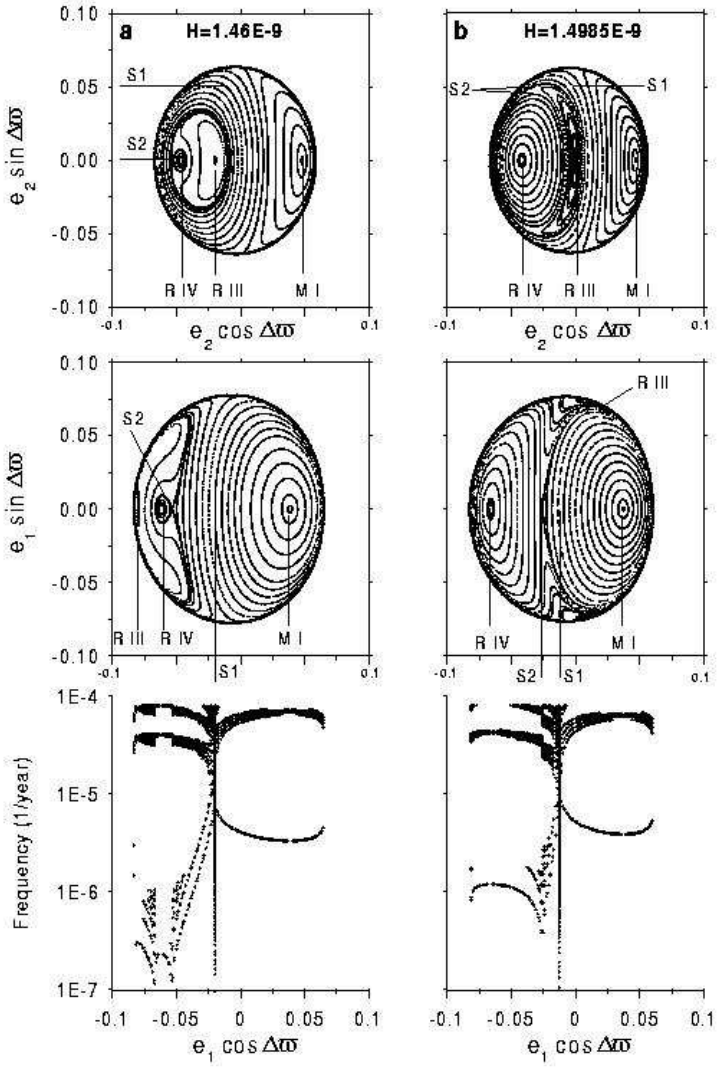

Figure 8: The same as in Fig. 2. a) Energy level g from Table I. b) Energy level h.

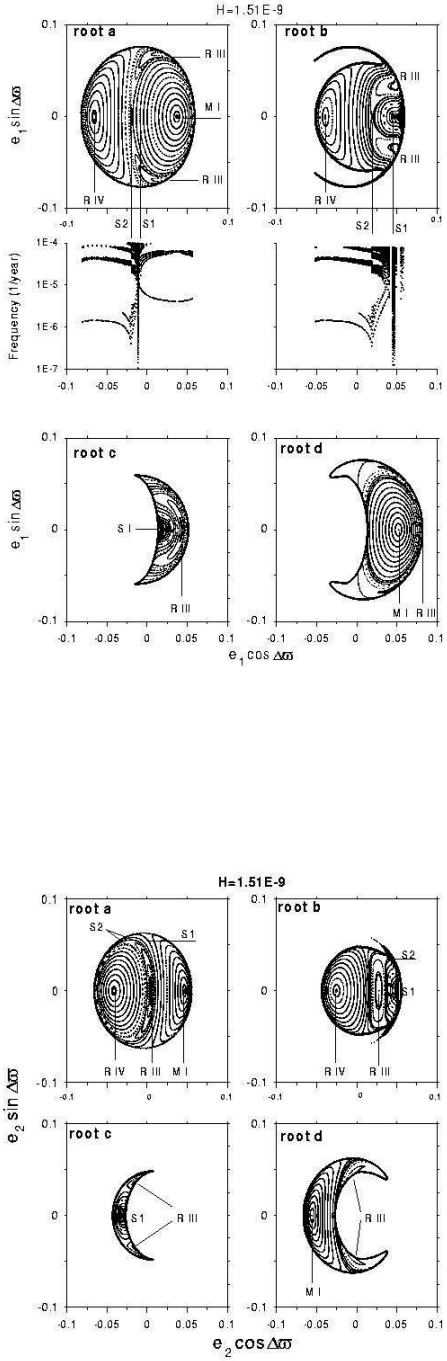

Figure 9: a) Uranus sections and spectral maps over energy level i. Top: surfaces of section of the kind a (left) and b (right). Middle: spectral maps corresponding to the sections a (left) and b (right). Bottom: Surfaces of section of the kind c (left) and d (right). b) Neptune surfaces of section corresponding to sections given in figure a). Top: sections a (left) and b (right). Bottom: sections c (left) and d (right).

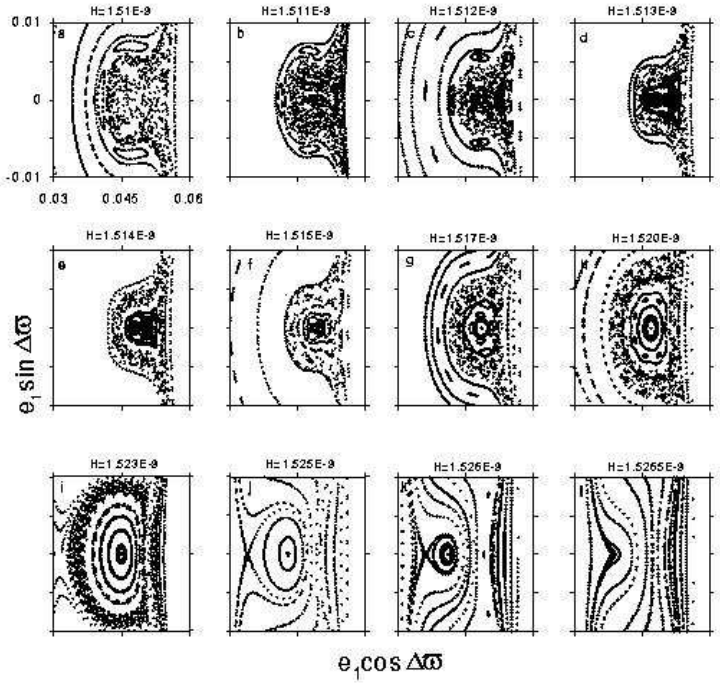

Figure 10: The enlarged domains of Regime V of motion. At $H \approx +1.511 \times 10^{-9}$ (b), a complex dynamical structure arises in the phase space, which survives up to $H \approx +1.514 \times 10^{-9}$ (10e). The nature of this structure was not studied in detail, but it probably involves secondary resonances. For $H \approx +1.517 \times 10^{-9}$ a new robust mode of motion appears, the Regime V.

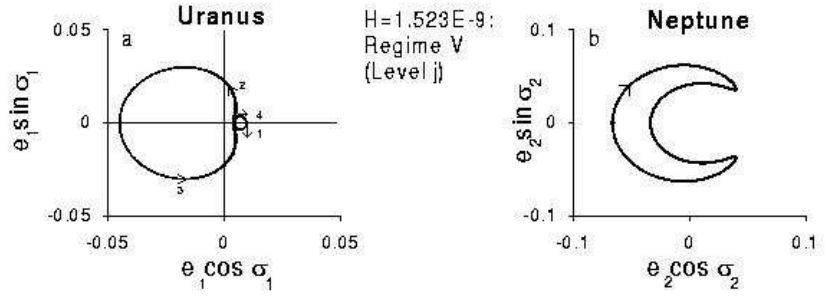

Figure 11: Example of the resonant motion in Regime V: (a) periodic orbit of Uranus, (b) periodic orbit of Neptune. Points show initial positions of the planets, and arrows show the direction of motion. In figure a, numbers 1-4 represent four steps of simulation, in which σ_1 begins with retrograde circulation (1), evolves in a direct circulation (2,3), and returns to retrograde circulation (4). The energy corresponds to level j from Table I.

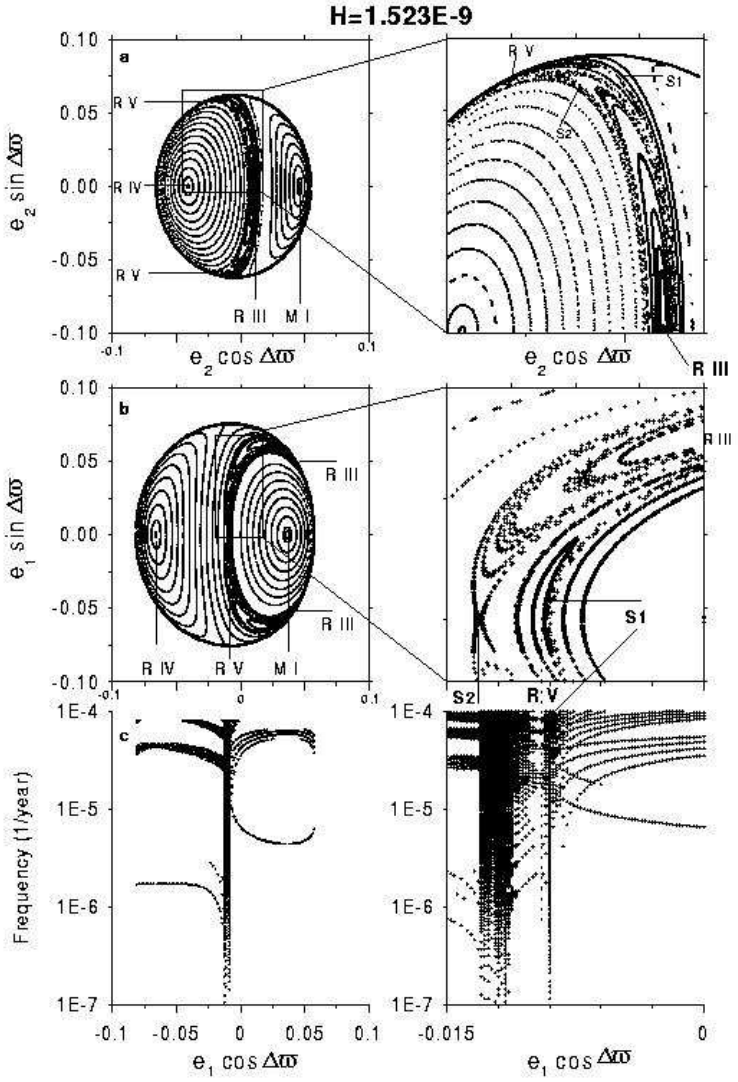

Figure 12: a) Surfaces of section of Neptune. b) Surfaces of section of Uranus. c) Spectral maps corresponding to the solutions shown on the Uranus section. The main regimes of motion are indicated on the sections. Energy level j from Table I. Panels on the right-hand side are the enlarged regions of the figures a, b and c.

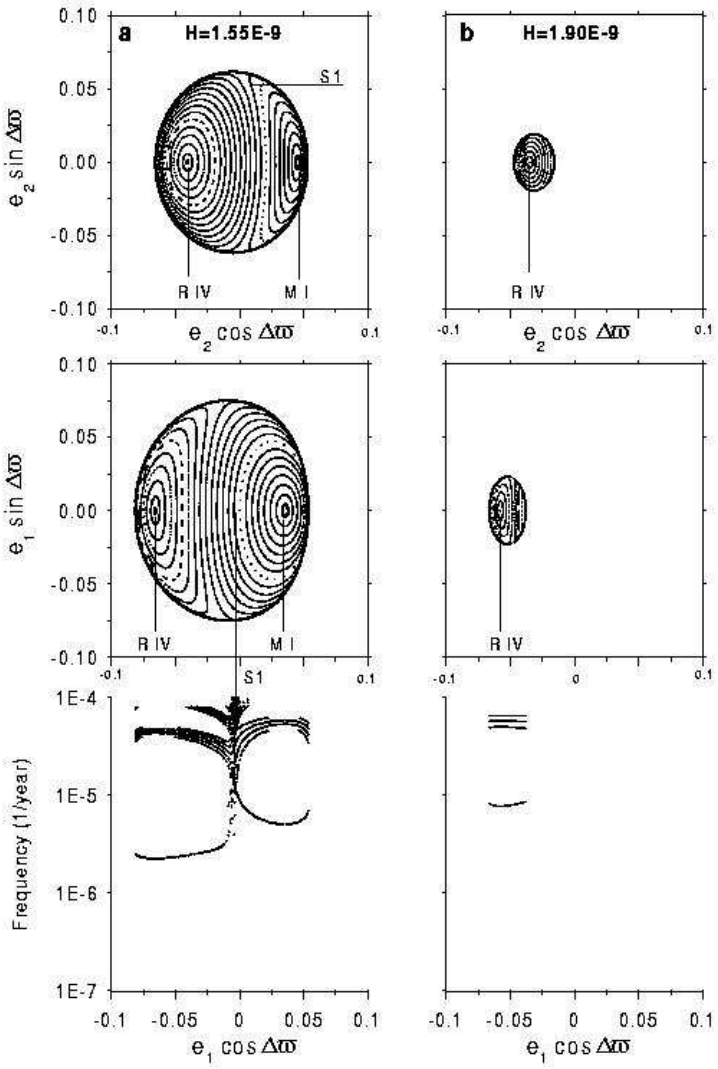

Figure 13: The same as in Fig. 2. a) Energy level k from Table I. b) Energy level l. Scale and axes are the same in both figures.

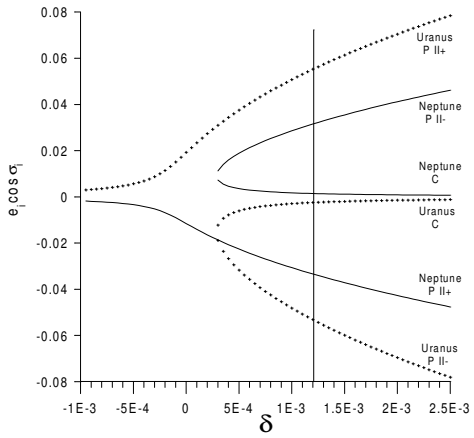

Figure 14: Coordinates of the three zero-gradient points C, PII$^-$ and PII$^+$ of the Hamiltonian (11) as a function of δ. The condition $e_i < 0$ means that $\sigma_i = \pi$ and $e_i > 0$ means that $\sigma_i = 0, i = 1, 2$. The coordinates of the points C, PII$^-$ and PII$^+$ shown in Fig. 1, are indicated by vertical line, for $\delta = 0.0012$.

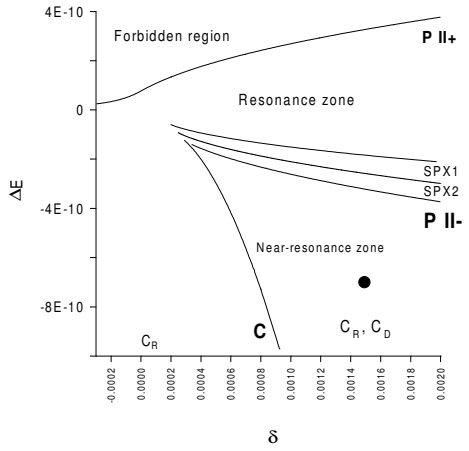

Figure 15: The (δ,ΔE) parameter plane. The resonance zone is located between curves PII$^+$ and PII$^-$, and the near-resonance zone between PII$^-$ and C. C$_R$: retrograde circulation, C$_D$: direct circulation. Full circle represents the actual position of the Uranus-Neptune system.

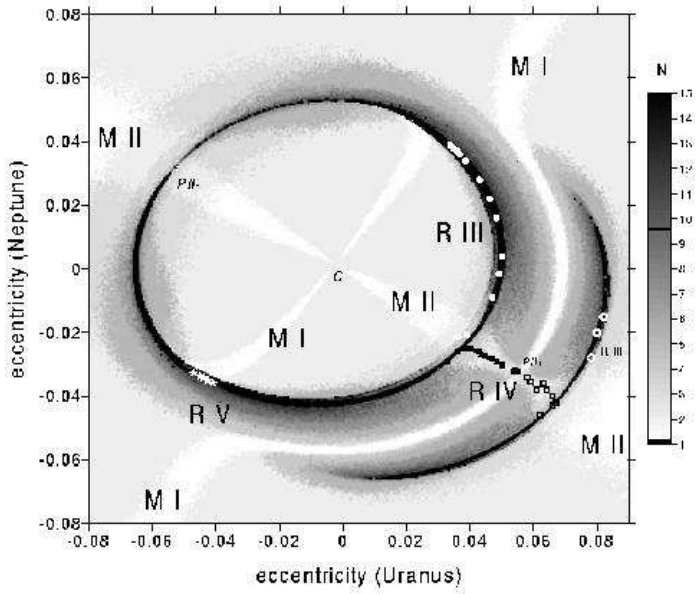

Figure 16: The dynamical map of the representative plane of initial conditions, for $\delta = 0.0012$. The labels represent the main regimes of motion. Full symbols represent some initial conditions of the periodic orbits obtained from sections b, while open symbols represent the same orbits obtained from sections a (Callegari 2003). Circles: R III, squares: R IV, stars: R V. The location of the points PII^{+}, PII^{-} and C shown in Fig. 1 is also indicated.